Sensing and Bio-Sensing Research 37 (2022) 100517

Contents lists available at ScienceDirect

Sensing and Bio-Sensing Research

journal homepage: www.elsevier.com/locate/sbsr

# Viral particles imaging through evanescent wave scattering in a total internal reflection laser microscope

Roberto Lo Savio [a], Sara Piselli [a], Cinzia Bertelli [b], Massimo Pizzato [b], Adolfo Carloni [a,*]

[a] NTP Nano Tech Projects SRL, Via Circonvallazione 11/A, 61048 Sant'Angelo in Vado, Italy
[b] Department of Cellular, Computational and Integrative Biology (CIBIO), University of Trento, 38123 Trento, Italy

ARTICLE INFO

*Keywords:*
Microscopy
Scattering
Nanoparticles
Virus
Biosensing

ABSTRACT

Optical imaging of objects at the nanometric scale is limited by light diffraction, and for this reason several sub-diffractive optical microscopy techniques have been developed in the last decades. In this article we present an optical laser microscope specifically designed for detection of nano-materials exploiting the Mie scattering between the evanescent wave generated by a laser beam travelling in a transparent substrate through total internal reflection and the nano-objects deposited on the substrate itself. The setup, including the laser source, can be fully integrated inside an optical microscope requiring only a geometric alignment with the substrate thus reducing the complexity and the cost. We also report two possible applications: quantitative detection of Au nanoparticles in the 20-100 nm size range and semi-quantitative detection of virions immobilized on the substrate through bioreceptor / antigen binding, including, but not limited to, SARS-CoV-2. A minimum virus amount of $\approx 10^5$ in the reaction volume is observed. The results presented here open the route towards unprecedent applications in molecular biology or molecular diagnostics.

## 1. Introduction

The detection and characterization of single particles at the nanoscale level is important in several field applications, from materials science to biology, and for this purpose several techniques were developed and are now well established: some of them investigate the collective properties of nanomaterials, such as dynamic light scattering, x-ray spectroscopy or diffraction, optical spectroscopy (absorption/transmission, photoluminescence); others investigate individual properties of single nanoparticles, such as atomic force microscopy or electron microscopy.

One of the most demanding challenges when dealing with nanomaterials is that standard imaging optical techniques using visible wavelength cannot be used due to diffraction limits.

Several techniques based on fluorescence imaging have been developed to overcome this limitation: widefield microscopy, total internal reflection microscopy, confocal microscopy, light sheet microscopy, two-photon microscopy, etc. [1,2,3,4,5]. Fluorescence microscopy provides a high contrast image in which the signal given by the fluorophores is superimposed over a perfectly black background; moreover, the possibility to use several fluorophores can add a second layer of information provided by the colour [6]. However, in recent years new imaging techniques based on scattering rather than fluorescence have been developed: total internal reflection scattering microscopy (TIRSM), interferometric scattering microscopy, differential interference contrast microscopy [7,8,9,10]. In fact, in spite of the wide diffusion of fluorescence-based microscopy, scattering has several advantages, as a physical process, when compared to fluorescence.

1) Scattering is more efficient, given the higher cross section: as an example, the scattering cross section of a single 50 nm gold sphere at 520 nm is around $10^{-11}$ $cm^{-2}$ [11], which is at least three orders of magnitude higher than absorption cross sections of typical fluorescence dyes, in the $10^{-16}$ $cm^{-2}$ range [12,13].

2) Scattering efficiency of nanoparticles can be tuned by controlling the shape (sphere, cubes, cages etc.), the composition (gold, silver, organic, core/shell, etc.), and the local refractive index near the particle surface [14]. These properties, paired with a simple but keen laser coupling system, makes them ideally suited for extremely sensitive diagnostic devices in a very broad optical range. Vice versa the excitation wavelength of the optical system and the absorption wavelengths of the fluorophore cannot be perfectly matched.

3) Nanoparticles offer great perspectives in a chemical process, since

* Corresponding author.
*E-mail address:* a.carloni@ntpsrl.biz (A. Carloni).

https://doi.org/10.1016/j.sbsr.2022.100517
Received 18 May 2022; Received in revised form 5 August 2022; Accepted 9 August 2022
Available online 12 August 2022
2214-1804/© 2022 The Authors. Published by Elsevier B.V. This is an open access article under the CC BY license (http://creativecommons.org/licenses/by/4.0/).

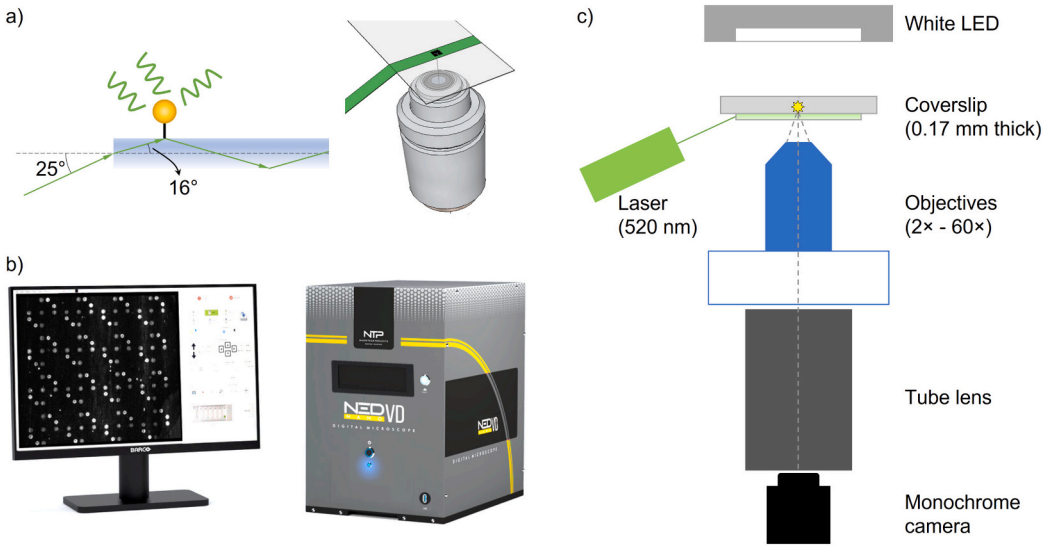


**Fig. 1.** NED-VD setup; a) the laser light hits the edge of the coverslip at 25° and is confined inside the glass through total internal reflection; the light is scattered by the nano-materials on the surface and is collected by the objective. b) Photograph of the NED-VD device. c) Overview of the optical setup.

they can be properly engineered and employed as carriers for multiple bioreceptors bio-conjugated on their external surface, thus increasing the overall sensing properties in the assay [15]. This is not true for fluorescent molecules which can bind only one-to-one to each analyte.

4) Fluorescence signals are intrinsically subjected to photobleaching effect and this can affect both the robustness and the stability of the detected signal, and the repeatability of the measurement. On the other side, the fraction of light scattered from a metal nanoparticle is constant, since it is less prone to damaging and/or modification due to laser illumination.

Here we describe a full digital device, called Nano Eye Device – Virus Detector (NED-VD), which is an optical inverted laser microscope designed for the observation of nanomaterials and nanoparticles through scattering. The laser excitation system, based on a patented technology [16], allows to generate an evanescent wave close to the substrate surface thanks to total internal reflection, achieved by simple geometry between the laser beam and the substrate itself; the nano-objects immobilized close to the substrate surface scatter the light that can be finally collected by the microscope objective. Further details are reported in the Experimental Section. Despite the underlying physical principle being the same, there are two main differences comparing with total internal reflection scattering microscopy: the excitation scheme is much simpler, not requiring any additional optical element between the laser source, the substrate, and the collection optics, and the sample can be analyzed also in air without using liquid interfaces.

Its simplicity, combined with potential high sensitivity, up to single particle, makes it interesting for molecular diagnostics since it allows the detection of both inorganic (i.e., Au nanoparticles used as biomarkers) and organic (i.e., viruses) particles at very low cost. This system allows for a considerable reduction in the size and complexity of laser-based microscopes and related applications, especially for nanoparticles detection and related optical biosensing.

Compared to other elastic scattering-based techniques, such as dark-field microscopy, the use of evanescent wave as excitation source guarantees that only the objects close to the substrate surface contribute to the detected signal.

The working principle of this technology is demonstrated through the detection of sub-diffractive functionalized AuNP, and as possible biosensing application we report the label-free detection of spherical viruses, also including SARS-CoV-2, through bioreceptor/antigen interaction.

## 2. Experimental section

### 2.1. NED-VD device

The main goal of NED-VD device is to simplify the process of detection of nano objects through optical imaging: to this end, the instrument is equipped only with a optical laser coupling method emitting a line-shaped laser beam in the visible range, an air-lens objective, and a monochromatic camera.

Thanks to this simplified optical setup and to the small size of the required components, the laser coupling method is inserted inside a multi-objective (up to 6) microscope setup in order to have two alternative illumination methods: standard white light transmission mode, and laser evanescent wave mode, sensitive to the substrate surface (Fig. 1).

The core of this optical coupling system is composed of a 520 nm semi-telecentric laser line generator (Schäfter+Kirchhoff, model number 5LTM-250-11 + 55CM-520-48-O08-A7.5-P-6) focused on the edge of a thin transparent substrate (i.e., a standard 0.17 mm-thick glass coverslip) with an angle of incidence of 25° between the laser beam and the horizontal plane. The laser is focused at a distance of 245 mm (depth of focus of 145 mm), and the distance between the laser and the coverslip edge is 250 mm. The laser line has a width of 4.8 mm and a height of 0.196 mm, thus guaranteeing a complete illumination of the coverslip edge.

The 25° incidence angle is properly chosen in order to achieve internal reflection of the laser light inside the substrate and can be slightly tuned for image optimization, within a +/− 2° tolerance, depending on the substrate refractive index.

The NED-VD is equipped with six semi-apochromat objectives (UIS2, Olympus UPLFLN series) on an automated revolver, spanning from 2× to 60×. The images are collected by a monochrome camera (IDS UI-3280CP-M-GL), using an exposure time of 200 ms.

The electronical part consists of a dedicated and custom developed motherboard (2.4 GHz processor, 8 GB RAM) able to control the camera, the objectives, the slide movements in XY axes, the focus in Z axis, and the light sources.

In NED-VD, since the substrate itself acts as a waveguide, when the laser beam hits the edges, an evanescent wave field is generated at the interface and propagates above the surface: considering a laser wavelength of 520 nm, a glass refractive index of 1.47, and an incidence angle of 25° the resulting penetration depth is 42 nm. Thus, any nano-object

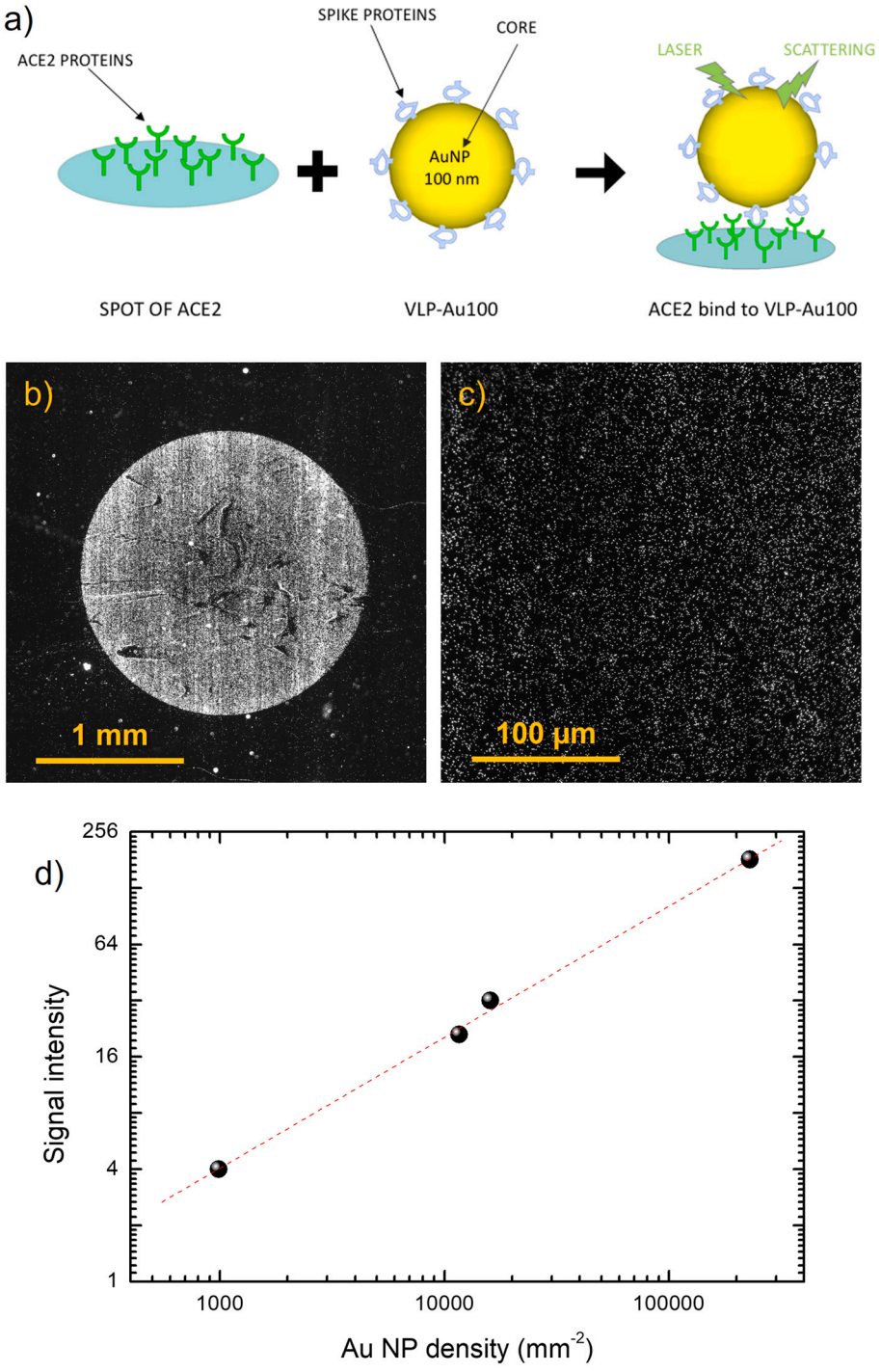


**Fig. 2.** Detection of 100 nm-sized gold nanoparticles functionalized with SARS.CoV.2 spikes and then captured by ACE-2 on slide. a) Scheme depicting the immobilization of Au NPs on the spot region. b) NED-VD image of a spot filled with Au NPs acquired at 4× magnification. c) Central region of the spot acquired with NED-VD at 40×. d) Graph showing the correlation between the surface density of Au NPs and the signal intensity (dashed red line is a guide to the eye); signal intensity is obtained from 8-bit monochromatic images (values in the 0–255 range). (For interpretation of the references to colour in this figure legend, the reader is referred to the web version of this article.)

immobilized on the substrate surface will scatter the laser light that can be collected by the microscope objective on its vertical (Fig. 1). The entire microscope is enclosed in a benchtop instrument.

### 2.2. Substrate functionalization

Glass coverslips (60 × 24 mm, 0.17 mm thickness) functionalized with aldehydic groups were purchased from Schott-Nexterion.

The bioreceptors used to define the active regions on the substrate are angiotensin-converting enzyme 2 (ACE2) (Signal-Chem, concentration 0.2 µg/µL), or a monoclonal antibody against the spike protein of SARS-CoV-2, referred as "antispike" in the following (Signal-Chem, concentration 0.5 µg/µL). Bioreceptor concentration has been chosen after investigating its effect on the assay performances. In particular, a wider range between 0.05 and 1.0 µg/µL has been explored showing an increasing trend up to 0.2 µg/µL, followed by a saturation behavior. Bioreceptors were dispensed without further dilution on the coverslip surface by drop casting through manual deposition. The drops were allowed to dry at 25 °C while shaking the coverslip at 1200 rpm in a thermo-shaker (Bio-San PST-100HL): after drying, a circular spot is formed, defining the active area on the coverslip. The drop volume determines the spot size, varying between 0.3 and 1.0 µL with corresponding spot size was in the range of 1–2 mm. The estimated nominal surface concentration of bioreceptors in the active spot area slightly

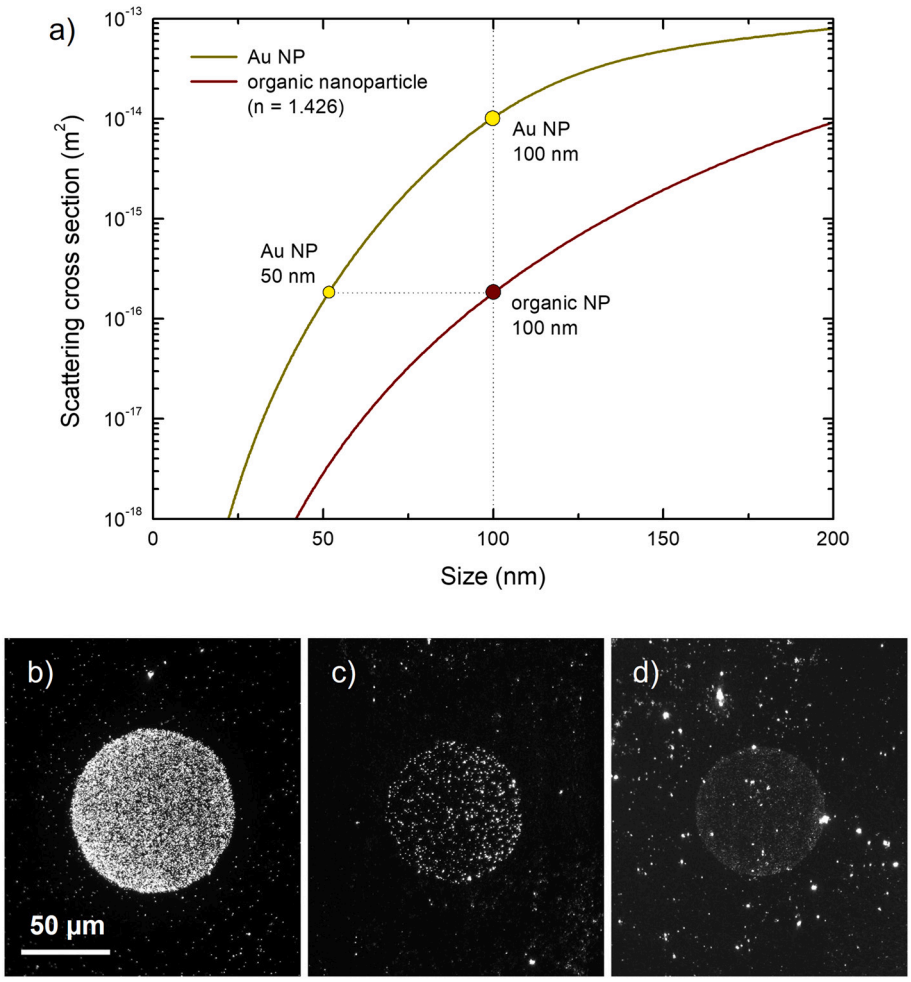


**Fig. 3.** a) Scattering cross section of spherical gold (yellow) and organic (red) nanoparticles; the refractive index used for organic nanoparticle is compatible with that of viral particles. b-d) NED-VD images of Au NPs of 100, 50, and 20 nm respectively (the scale bar is the same). Due to the lower intensity the image in d) is acquired by increasing the digital gain of the camera. The three images have been acquired using the same 40× objective. (For interpretation of the references to colour in this figure legend, the reader is referred to the web version of this article.)

varied between 2.5 and 3.0 × $10^{11}$ / $mm^2$. This represents an upper limit estimation only based on the number of bioreceptors deposited on the substrate; due to deposition method a random orientation is expected, thus reducing the amount available for further interactions. However, the bioreceptor-substrate interaction and the use of additional, more efficient, deposition methods is beyond the scope of this paper.

After bio-receptor dispensing the coverslips were stored at 4 °C.

### 2.3. Au nanoparticles preparation

AuNP (20, 50, and 100 nm size) functionalized with NHS groups were purchased from Cytodiagnostics; they were bio-conjugated with commercial spike proteins (Signal-Chem, concentration 0.2 µg/µL) using the protocol provided by the supplier.

### 2.4. Virus production

To assess the ability of NED-VD to detect virions, HIV-1 pseudotyped with the SARS-CoV-2 Spike protein was produced in HEK293T cells. For safety reasons, a HIV-1 molecular clone (*env*-defective pNL4–3), limited to single cycle replication was used. Briefly, 3.5 million HEK293T cells were seeded in 10 cm plates and transfected, by calcium-phosphate method, with 17.5 µg of pNL4–3 *env*- and 2.5 µg of pcDNA3.1 encoding SARS-CoV-2 spike, bearing a premature stop codon within the C-terminal tail. To control the specificity of NED-VD, in parallel, pNL4–3 *env*- was complemented with 2.5 µg of empty pcDNA3.1; alternatively, pNL4–3 *env*- was substituted with 17.5 µg of a NL4–3 variant harboring three stop codons within *gag*, making the construct unable to produce viral particles. Two days after transfection, the virions-containing cell supernatant was clarified by centrifugation (2500 rpm, 5 min) and passed through filters with 0.45 µm pores. Pseudotyped HIV-1 was then purified by overlay on a 25% sucrose cushion and ultracentrifugation (100.000 ×*g*, 2 h). Eventually, the viral particle content of the purified virions preparation was assessed by RT-assay (SG-PERT), as previously described [17] while the concentration was evaluated by detection of the viral genomic RNA by qPCR.

As an alternative virus model, we also used original SARS-CoV-2. To produce a stock preparation of SARS-CoV-2, a confluent plate of VERO E6 cells was infected with SARS-CoV-2 at 0.01 MOI [18]. Four days after infection, the cell culture supernatant, containing SARS-CoV-2 was collected and centrifuged (1200 rpm, 5 min) and filtered to remove cell debris. SARS-CoV-2 was then concentrated by overnight centrifugation (3000 rpm at 12 °C). The final virus preparation was quantified by qPCR (Liferiver 2019-nCoV Real Time Multiplex RT-PCR Kit) and by plaque assay, as described previously [19], and resulting values are 3 × $10^{10}$ genomes/mL and 3 × $10^4$ pfu/mL.

### 2.5. AuNP and virions assay

The experiments were performed using glass coverslips divided in 12 separated cylindrical wells (diameter 6 mm, maximum volume 150 µL) using a silicone isolator gasket and a multi-well chamber (both purchased from Grace Biolabs).

To capture nanomaterials, first the coverslip regions outside the spot were blocked in order to prevent non-specific adhesion, then the suspension containing the Au NPs was dispensed and incubated, and finally

the coverslips were washed to remove unbound nanoparticles.

In the pre-reaction step, each well was covered with 50 μL of blocking solution (PBS, 1% BSA, 0.05% Tween-20) and the entire reaction chamber was incubated in a thermo-shaker (Bio-San PST-100HL) for 15 min at 25 °C with 250 rpm agitation. Subsequently, every well was washed at room temperature twice with 100 μL of a wash buffer (PBS, 0.05% Tween-20).

In the reaction, 20 μL of solution containing nanomaterials (Au NPs or virions) was added to each well and the entire reaction chamber was incubated in the same thermo-shaker for 30 min at 34 °C with agitation at 1000 rpm. The reaction solution was then removed, and each well was washed at room temperature twice with the same wash buffer used previously to eliminate the residual nano-materials that did not bind to bio-receptor spots. Finally, the isolating gasket was removed, and the glass coverslips were washed again in a 50 mL tube with distilled water for 3 min at room temperature. After this last step the coverslip was dried with compressed air before being analyzed with NED-VD.

## 3. Results and discussion

### 3.1. Detection of gold nanoparticles by NED-VD

Gold nanoparticles (100 nm size) bio-conjugated with spike proteins from SARS-CoV-2 virus were deposited on the ACE2 spots following the protocol described in materials and methods. The spots were then visualized with the NED-VD device and two representative images acquired at different magnification are shown in Fig. 2b and c. While at low magnification the spot appears as a homogeneous white area on a dark background, increasing the magnification allows to resolve the single nanoparticles.

For biosensing applications quantitative analyses are important, and the relevant information is the number of Au NPs docked into the spot region, rather than simple signal intensity, since it usually relates to the number of analytes. The number of Au NPs can be measured from images using thresholding algorithms that can separate the NPs from the background [20], provided that the Au NPs are spatially resolved and isolated: for magnification higher than 40× this typically occurs for densities lower than $3 \times 10^5$ NP/mm$^2$. However, when the density is too high and/or when low magnification is used, it is necessary to rely on indirect measurements. Due to the illumination scheme with the evanescent wave close to the coverslip surface, each Au NP has a similar intensity, and this guarantees a reliable direct proportionality between the surface density of Au NP on the spot and the signal intensity, as shown by the correlation between the two parameters shown in Fig. 2d. In both cases the values are obtained by subtracting from the values obtained inside the spot those obtained in the area surrounding the spot. In this way we consider spurious the signals due to impurities and/or to non-specific adhesion of Au NPs outside the spot region. The curve shown in Fig. 2d can be considered as a calibration curve between the scattered signal and the surface density of scattering centers; since the light intensity depends on several parameters such as laser power and the camera acquisition parameters (exposure time, digital gain) it is necessary to build different calibration curves for different combinations of such parameters.

The possibility to correlate direct (surface density) and indirect (intensity) measurements is very useful for large scale applications where it is more convenient to scan the coverslip surface quickly. The minimum number of Au NPs detectable depends on the assay and the protocol used since they influence the rate of specific adhesion of Au NPs on the spot region and the non-specific binding on the glass. In the assay presented here, a minimum surface density of ≈500 NPs/mm$^2$ is achieved. This is an indication of the sensitivity of the optical device only; for biosensing applications the sensitivity is mostly given by the efficiency of the assay and specifically by the fraction of analytes that is docked into the spot area.

To evaluate the performances of NED-VD in a broader range of

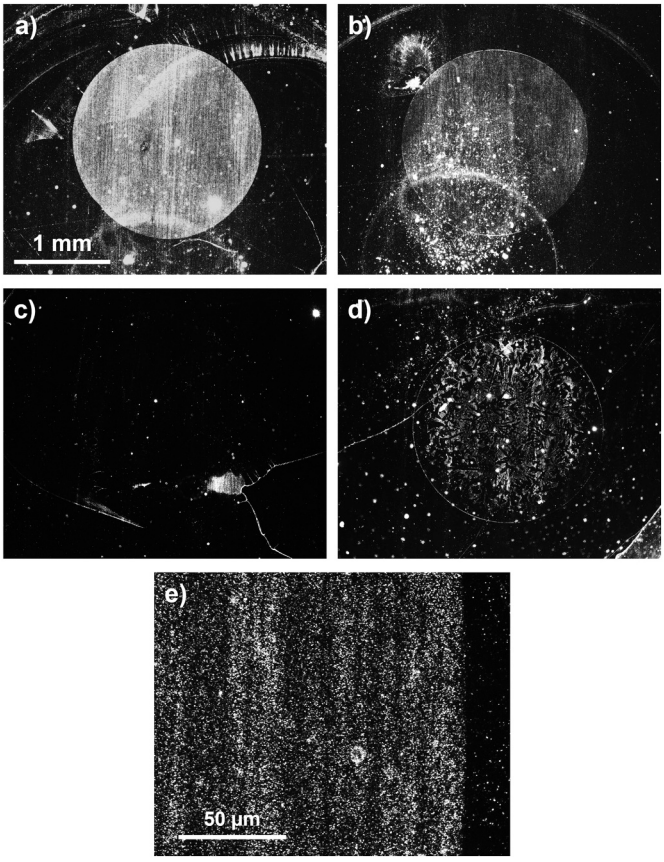


**Fig. 4.** Comparison between ACE2 and anti-spike monoclonal antigen: spot observed at 4× magnification after incubation of $5 \times 10^6$ virions on ACE2 (a) and anti-spike (b), and corresponding negative controls (c, d); scale bar is the same in all four images; e) 40× magnification image of the right edge of the spot in panel a).

situations, Au NPs of different sizes were tested, from 20 nm to 100 nm; the scattering cross section was found to decrease by four orders of magnitude, passing from 100 to 20 nm (Fig. 3a), confirming that while the amount of light scattered by nano-objects depends on several parameters (laser wavelength, material, surrounding medium, shape and size, etc.) size is the most influent.

In Figs. 3(b-d) three images of spots obtained incubating the same amount of Au NPs in the reaction well are shown: despite a dramatic intensity decrease, NED-VD is capable to detect Au NPs up to 20 nm, although in this case it is not possible to quantitatively count single particles. Due to the strong size dependence of scattering cross section and the very low signal provided by 20 nm Au NPs we can guess that this represents the minimum detectable size. The possibility to visualize objects with low scattering cross section opens the route towards the detection of organic nano-objects, such as viruses or bacteria, whose scattering cross section is much lower compared to metal nanoparticles of similar size. Fig. 3a shows the cross section of a quasi-spherical virus lentiviral particle pseudotyped with the SARS-CoV-2 spike of a size of ≈ 100 nm (like Influenza virus, HIV, coronaviruses, etc.) which is comparable to that of Au NPs having a size of 50 nm. This result indicates that authentic viruses can be detected by NED-VD.

### 3.2. Detection of viral particles by NED-VD

Having demonstrated that Au NPs up to 20 nm in size can be visualized by NED-VD, of the instrument was tested for the detection of HIV-1 viral particles pseudotyped with the SARS-CoV-2 spike protein in order to exploit the same bioreceptor/antigen interaction. Pseudotyped HIV-1

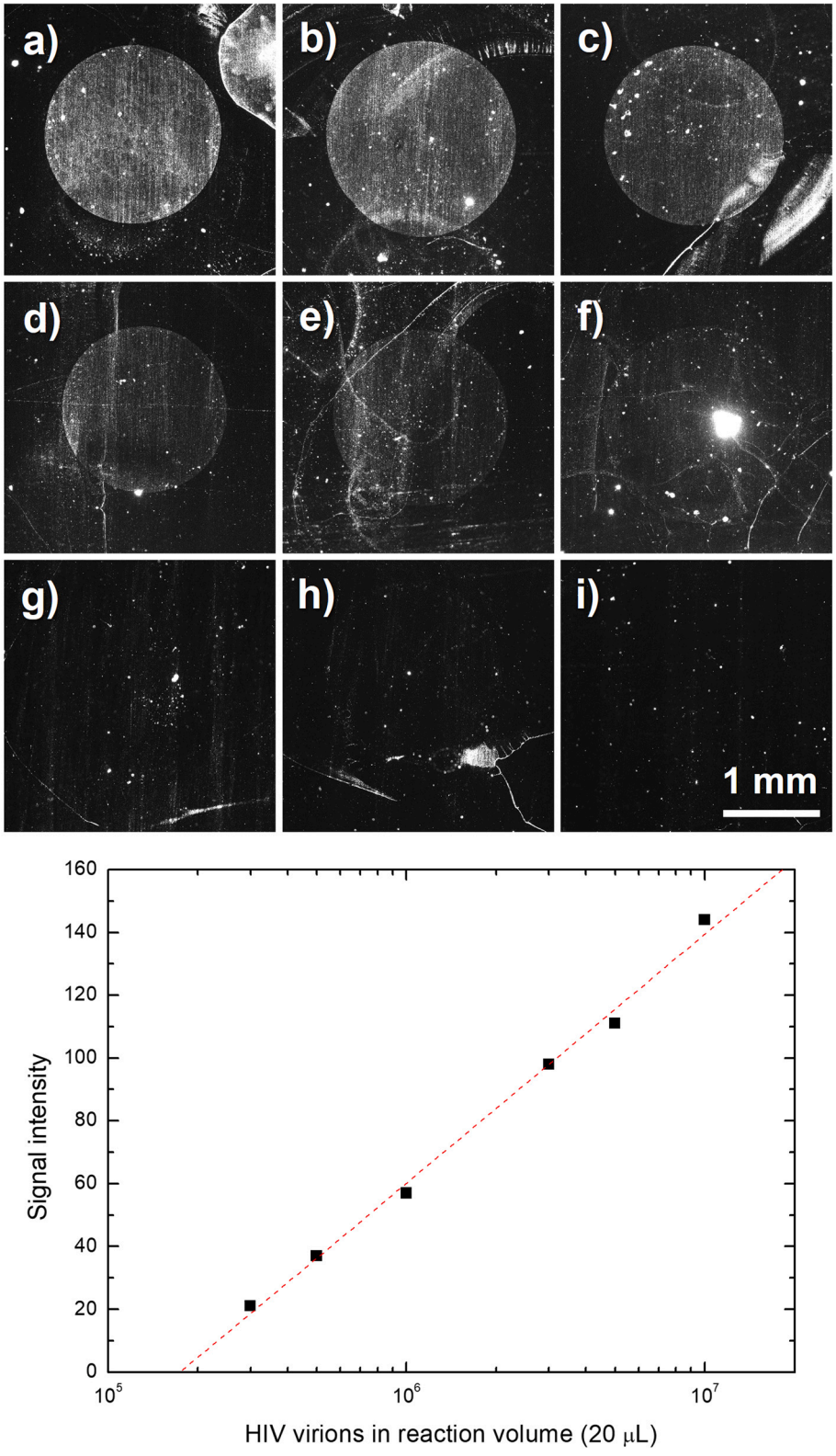


**Fig. 5.** a-f) NED-VD images of spots observed at 4× magnification after incubation with different SARS-CoV-2 pseudotyped HIV-1 virions amount: $10,^{7}$ $5 \times 10,^{6}$ $3 \times 10,^{6}$ $10,^{6}$ $5 \times 10,^{5}$ $3 \times 10.^{5}$ The bright spot in f is due to a dust particle. g-i) NED-VD images of negative controls. j) pseudotyped HIV-1 dilution curve; the red line is an apparent linear fit.

virions were incubated on the coverslip following the protocol described in the experimental section.

Although TIRSM has been used for the detection of viral genome [21], our purpose here is the detection of the intact whole virus. A series of experiments were carried out to compare the suitability of two different kinds of bioreceptors, ACE2 and an anti-spike monoclonal antibody (Fig. 4). In both cases a solution, containing $5 \times 10^6$ virions, was incubated, and the spots were clearly visible (Fig. 4a, b) with a

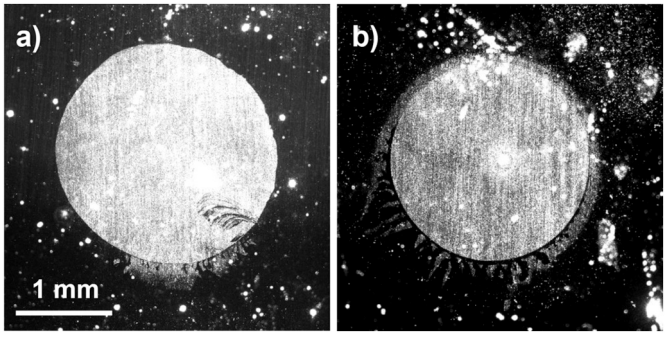


**Fig. 6.** Low magnification imaging of two spots at 4× magnification after incubation with $10^7$ virions of SARS-CoV-2 (a), and (b) HIV pseudotyped with SARS-CoV-2 spike. The scale bar is the same.

higher intensity in the ACE2 spot. At the same time, negative controls containing only DMEM were incubated following the same protocol and produced no specific signal on the ACE2 spot (Fig. 4c); specific signal generated by virus particles is easily distinguished from impurities and residual salts that can be present in the solution containing the anti-spike monoclonal antibody (Fig. 4d). We believe that this difference is mostly related to the immobilization of the bioreceptor on the substrate rather than the interaction with the analyte. This aspect will be investigated more in detail in the future.

Moreover the using of ACE2 as bioreceptor is most suitable in view of possible diagnostic applications since the interaction between a specifically designed anti-spike bioreceptor would be more sensitive to the modification of spike protein in different SARS-CoV-2 variants requiring continuous update of bioreceptor design.

Given the higher performance of ACE2 both in terms of signal intensity and absence of impurities, we will consider only ACE2 as bioreceptor in the following.

Inspecting the spot at higher magnification reveals the granular pattern of the signal, due to single virions (Fig. 4e). In contrast to what observed for Au NPs, the virions do not exhibit the same isotropic scattered light intensity. This can be explained by several factors, such as a non-homogenous size distribution and/or non-spherical surface.

Serial dilutions of pseudotyped HIV-1 samples were produced to determine the minimum detectable concentration by the assay (Fig. 5). A linear trend in a semi-logarithmic chart was observed throughout the analyzed range (two orders of magnitude), from which it is possible to estimate a minimum detectable concentration of $\approx 2 \times 10^5$ viruses / 20 μL that is a 3000-fold dilution of the starting concentration obtained after virus cultivation ($3 \times 10^4$ pfu/mL). This value is comparable to that observed in TIRFM detection of influenzavirus [22] and human cytomegalovirus [23], or reflectance microscopy of Ebola-like virus [24]. The minimum detected amount is comparable also with that observed in several assays detecting influenzavirus and coronavirus based on surface-enhanced Raman scattering techniques [25], with LODs between 50 and $10^6$ PFU/mL.

We observed similar using SARS-CoV-2 virions, as shown in Fig. 6, where two spots were obtained by incubating the same amount ($10^7$) of both pseudotyped HIV-1 and SARS-CoV-2 virus.

This experimental result confirms that NED-VD can be used to detect different enveloped viruses, belonging to different families and with capsids of different symmetry, provided that their size and shape guarantees sufficient light scattering. For the same reason, it is plausible that only viruses preserving their structure can be detected using this method since bioreceptor/antigen interaction is necessary but not sufficient condition: spherical shape and size larger than 50 nm are tight requirements. The possibility to selectively detect only intact and active viruses would be interesting for possible application since the device presented here could support other techniques that detect only the virus genome (qPCR) and could be a faster alternative to plaque assays.

In order to lower the assay sensitivity further improvements are necessary, especially in the bioreceptor-antigen interaction: other bioreceptors having higher affinity could be tested, their surface concentration can be tuned, orientation and adhesion could be controlled through protocol modifications [26,27].

## 4. Conclusions

The laser optical microscope NED-VD presented here is capable to detect nano-materials docked on a transparent substrate using a simple excitation setup that makes the instrument a reliable and cheaper alternative to other imaging techniques, such as TIRSM. The possibility to detect Au NPs up to 20 nm opens the way to biosensing applications. In fact, an assay for the detection of spherical viruses with an average size of ≈100 nm (HIV pseudotyped with SARS-CoV-2 spike proteins, and whole SARS-CoV-2) is presented here. The assay shows a minimum sensitivity of $\approx 10^5$ virions in the reaction volume. With the specific example of SARS-CoV-2 this value is below the amount of virus copies that should be detected with standard antigen rapid tests, exploiting the same bioreceptor/antigen interaction, according to WHO [28]. However, contrarily to other kind of tests the NED-VD gives the possibility to detect the intact virion allowing a simpler correlation between the presence of the pathogen and the state of infection in the patient.

## CRediT authorship contribution statement

**Roberto Lo Savio:** Formal analysis, Data curation, Visualization, Writing – review & editing. **Sara Piselli:** Investigation. **Cinzia Bertelli:** Resources. **Massimo Pizzato:** Validation, Supervision. **Adolfo Carloni:** Conceptualization, Methodology, Writing – original draft, Project administration.

## Declaration of Competing Interest

No competing interests.

## Acknowledgements

Present study research was entirely funded by company NTP Nano Tech Projects srl during pandemic times. Efforts towards this study research became possible thanks to NTP's funders & stakeholders.

## References

[1] K.N. Fish, Total internal reflection fluorescence (TIRF) microscopy, Curr. Protoc. Cytom. 50 (2009) 12.18.1–12.18.13, https://doi.org/10.1002/0471142956.cy1218s50.
[2] C.A. Combs, H. Shroff, Fluorescence microscopy: a concise guide to current imaging methods, Curr. Protoc. Neurosci. 79 (2018) 2.1.1–2.1.25, https://doi.org/10.1002/cpns.29.
[3] J.W. Lichtman, J.A. Conchello, Fluorescence Microscopy, Nat. Methods 2 (2005) 910–919, https://doi.org/10.1038/nmeth817.
[4] R.M. Power, J. Huisken, A guide to light-sheet fluorescence microscopy for multiscale imaging, Nat. Methods 14 (2017) 360–373, https://doi.org/10.1038/nmeth.4224.
[5] F. Helmchen, W. Denk, Deep tissue two-photon microscopy, Nat. Methods 2 (2005) 932–940, https://doi.org/10.1038/nmeth818.
[6] M. Dickinson, G. Bearman, S. Tille, R. Lansford, S.E. Fraser, S.E., Multi-spectral imaging and linear Unmixing add a whole new dimension to laser scanning fluorescence microscopy, Biotechniques 31 (2001) (2001) 1272–1278, https://doi.org/10.2144/01316bt01.
[7] J. Lee, G.W. Kim, J.W. Ha, Single-particle spectroscopy and defocused imaging of anisotropic gold nanorods by total internal reflection scattering microscopy, Analyst 145 (2020) 6038–6044, https://doi.org/10.1039/D0AN01071E.
[8] Z. Ye, X. Wang, L. Xiao, Single-particle tracking with scattering-based optical microscopy, Anal. Chem. 91 (2019) 15327–15334, https://doi.org/10.1021/acs.analchem.9b02760.
[9] A. Rashidi, S. Domínguez-Medina, J. Yan, D.S. Efremenko, A.A. Vasilyeva, A. Doicu, T. Wriedt, C.L. Wirth, Developing scattering morphology resolved Total internal reflection microscopy (SMR-TIRM) for orientation detection of colloidal ellipsoids, Langmuir 36 (2020) 13041–13050, https://doi.org/10.1021/acs.langmuir.0c02482.

[10] H. He, J. Ren, A novel evanescent wave scattering imaging method for single gold particle, Talanta 77 (2008) 166–171, https://doi.org/10.1016/j.talanta.2008.05.059.
[11] M. Loumaigne, C. Midelet, T. Doussineau, P. Dugourd, R. Antoine, M. Stamboul, A. Débarre, M.H.V. Werts, Optical extinction and scattering cross sections of plasmonic nanoparticle dimers in aqueous suspension, Nanoscale 8 (2016) 6555–6570, https://doi.org/10.1039/C6NR00918B.
[12] L. Wang, A.K. Gaigalas, V. Reipa, Optical properties of AlexaTM 488 and cyTM5 immobilized on a glass surface, Biotechniques 38 (2005) 127–132, https://doi.org/10.2144/05381MT03.
[13] S. Kumar, A. Singh, V.R. Singh, J.B. George, J. Balaji, Saturation dynamics measures absolute cross section and generates contrast within a neuron, Biophys. J. 111 (2016) 1328–1336, https://doi.org/10.1016/j.bpj.2016.06.044.
[14] P.K. Jain, K.S. Lee, I.H. El-Sayed, M.A. El-Sayed, Calculated absorption and scattering properties of gold nanoparticles of different size, shape, and composition: applications in biological imaging and biomedicine, J. Phys. Chem. B 110 (2006) 7238–7248, https://doi.org/10.1021/jp057170o.
[15] B.A. Kairdolf, X. Qian, S. Nie, Bioconjugated nanoparticles for biosensing, in vivo imaging, and medical diagnostics, Anal. Chem. 89 (2017) 1015–1031, https://doi.org/10.1021/acs.analchem.6b04873.
[16] A. Carloni, Laser Optical Coupling for Nanoparticles Detection, Patent WO 2016/006006 A1 (2016).
[17] M. Pizzato, O. Erlwein, D. Bonsall, S. Kaye, D. Muir, M.O. McClure, A one-step SYBR green I-based product-enhanced reverse transcriptase assay for the quantitation of retroviruses in cell culture supernatants, J. Virol. Methods 156 (2009) 1–7, https://doi.org/10.1016/j.jviromet.2008.10.012.
[18] D. Licastro, S. Rajasekharan, S.D. Monego, L. Segat, P. D'Agaro, A. Marcello, Isolation and full-length genome characterization of SARS-CoV-2 from COVID-19 cases in northern Italy, J. Virol. 94 (2020), https://doi.org/10.1128/JVI.00543-20 e00543–20.
[19] J.B. Case, A.L. Bailey, A.S. Kim, R.E. Chen, M.S. Diamond, Growth, detection, quantification, and inactivation of SARS-CoV-2, Virology 548 (2020) 39–48, https://doi.org/10.1016/j.virol.2020.05.015.
[20] N. Otsu, A threshold selection method from gray-level histograms, IEEE Trans. Syst. Man Cybern. Syst. 9 (1979) 62–66, https://doi.org/10.1109/TSMC.1979.4310076.
[21] S. Lee, S.K. Chakkarapani, E.S. Yeung, S.H. Kang, Direct quantitative screening of influenza a virus without DNA amplification by single-particle dual-mode total internal reflection scattering, Biosens. Bioelectron. 87 (2016) 842–849, https://doi.org/10.1016/j.bios.2016.09.019.
[22] S. Enoki, R. Iino, N. Morone, K. Kaihatsu, S. Sakakihara, N. Kato, H. Noji, Label-free single-particle imaging of the influenza virus by objective-type Total internal reflection dark-field microscopy, PLoS One 7 (2012), e49208, https://doi.org/10.1371/journal.pone.0049208.
[23] Q. Wei, H. Qi, W. Luo, D. Tseng, S.J. Ki, Z. Wan, Z. Göröcs, L.A. Bentolila, T.T. Wu, R. Sun, A. Ozcan, Fluorescent imaging of single nanoparticles and viruses on a smart phone, ACS Nano 7 (2013) 9147–9155, https://doi.org/10.1021/nn4037706.
[24] S.M. Scherr, G.G. Daaboul, J. Trueb, D. Sevenler, H. Fawcett, B. Goldberg, J. H. Connor, M.S. Ünlu, Real-time capture and visualization of individual viruses in complex media, ACS Nano 10 (2016) 2827–2833, https://doi.org/10.1021/acsnano.5b07948.
[25] F. Saviñon-Flores, E. Méndez, M. López-Castaños, A. Carabarin-Lima, K.A. López-Castaños, M.A. González-Fuentes, A. Méndez-Albores, A review on SERS-based detection of human virus infections: influenza and coronavirus, Biosensors 11 (2021) 66, https://doi.org/10.3390/bios11030066.
[26] Y. Liu, J. Yu, Oriented immobilization of proteins on solid supports for use in biosensors and biochips: a review, Microchim. Acta 183 (2016) 1–19, https://doi.org/10.1007/s00604-015-1623-4.
[27] N.G. Welch, Orientation and characterization of immobilized antibodies for improved immunoassays, Biointerphases 12 (2017) 02D301, https://doi.org/10.1116/1.4978435.
[28] World Health Organization, Antigen-detection in the diagnosis of SARS-CoV-2 infection, in: WHO/2019-nCoV/Antigen_Detection/2021.1, 2021. https://apps.who.int/iris/handle/10665/345948.

**Roberto Lo Savio** (r.losavio@ntpsrl.biz) is graduated in physics with a PhD in material science received from University of Catania in 2009. He carried out many important scientific research activities in the field of nanomaterials, microscopy and photonics, in different national and international research centres. He is expert in the creation of optical setups for spectroscopic analysis of nanomaterials and devices with specific skills in the analysis of physical processes, image analysis and calibration curves. He is author of several (+50) scientific articles in the nanomaterials sectors and physical science.

**Sara Piselli** (s.piselli@ntpsrl.biz) graduated in Molecular Health Biology in 2017 at University of Urbino. She has a great propension to biochemistry and nanotechnology thanks to her intensive commitment and experience gained in the fields of molecular biology, virology and in experimental laboratory activities. She possesses specific skills in the research, optimization and development of biomolecular protocols for virus detection either in capture of whole virions, either in molecular diagnostics based on DNA hybridization interactions and on antigen/antibody affinities.

**Cinzia Bertelli** (cinzia.bertelli@unitn.it) received an MSc in Cellular and Molecular Biotechnology and a PhD in Biomolecular Sciences at the University of Trento, where she currently conducts her postdoctoral researcher in the Virus-cell Interaction group led by prof. Massimo Pizzato. Her research interests include the biology of retroviruses and RNA viruses and the activity of antiviral restriction factors. She developed assays and tools for the research of SARS-CoV-2 and for the investigation of humoral immunity against the pandemic coronavirus.

**Massimo Pizzato** (massimo.pizzato@unitn.it) is Professor of Microbiology at the University of Trento, Italy. His research focuses on the biology of viruses and the interaction of viruses with the host cells. He received his PhD in Virology at the Institute of Cancer Research, London UK, and continued his post-doctoral research activity at the Dana Farber Cancer Institute, Harvard USA. He became a group leader at the Imperial College London and continued his independent research at the University of Geneva, Switzerland, before moving to the University of Trento, Italy where he currently leads the Virus-Cell Interaction group. He made seminal discoveries in the field of retroviruses interaction with cells and restriction factors. Since the pandemic outbreak of SARS-CoV-2 he is the director of a regional diagnostic laboratory.

**Adolfo Carloni** (a.carloni@ntpsrl.biz) is Scientific Director of NTP Nano Tech Projects srl (Italy). He is MSc in Industrial Chemistry from 2004 at Bologna University, Italy. He received two PhDs, one in Chemistry at University of Firenze Italy in 2008, and one in Health at University of Cranfield UK in 2010. He is the inventor of the method of optical laser coupling to detect nanoparticles and his research activity focuses on biosensors and optical devices. His interests include optical materials, coatings, nanoparticles, surfaces functionalization and laser microscopy. He manages research, design, development, integration and verification of the overall biosensing system, leading colleagues specialized in biology, physics, and informatics.